Cement and Concrete Research 40 (2010) 517–525

Contents lists available at ScienceDirect

Cement and Concrete Research

journal homepage: http://ees.elsevier.com/CEMCON/default.asp

Micro-mechanical modelling of alkali–silica-reaction-induced degradation using the AMIE framework

Cyrille F. Dunant [a,*], Karen L. Scrivener [b]

[a] EPFL STI IMX LMC, MXF 210 (Bâtiment MXF), Station 12, CH-1015 Lausanne, Switzerland
[b] EPFL STI IMX LMC, MXG 232 (Bâtiment MXG), Station 12, CH-1015 Lausanne, Switzerland

ARTICLE INFO

Article history:
Received 31 October 2008
Accepted 21 July 2009

Keywords:
Alkali-Aggregate Reaction (ASR) (C)
XFEM (out category)
Long-Term Performance (C)
Mechanical Properties (C)
Modelling (E)

ABSTRACT

AMIE, a finite element/extended finite element framework, has been designed to provide the tools to run detailed microstructural simulations; this paper demonstrates the possibility of simulating the mechanisms underlying the alkali–silica-reaction (ASR). The numerical model presented provides a better understanding of experimental observations. Macroscopic free expansion and degradation of mechanical properties have been previously linked to the extent of reaction. The connection between microscopic and macroscopic measurements, simulated by the model, supports the hypothesis that damage is induced by growing gel pockets in the aggregates.

1. Introduction

The alkali–silica-reaction (ASR) is characterised by the breakdown of silanol bonds in poorly crystallised silica found in aggregates in the presence of alkaline ions. The product of this reaction is an amorphous alkali–silica "gel" which expands in the presence of moisture, inducing stress in the microstructure. This causes concrete expansion and mechanical properties degradation. Prediction of the free expansion, as well as the subsequent degradation of the stiffness and strength are of great importance for the owners and managers of affected structures.

Mechanical modelling of ASR at the material level poses significant challenges both technical and scientific. A model based on physics is necessary to understand the degradation mechanism and to permit prognosis and life-time assessment of affected structures. Such a model should be based on a detailed meso-mechanical representation of the concrete microstructure to capture the variety of mineralogies found in the field.

In this paper, we present a micro-mechanical model of ASR implemented using a purpose-developed extended finite element modelling (XFEM) framework capable of a full scale simulation of laboratory-sized samples in two dimensions. This framework called AMIE (automated mechanics for integrated experiments) was developed to be very flexible to enable study of various proposed ASR mechanisms at the meso-structural level [1,2]. Ben Haha and colleagues proposed a method to measure the advancement of the reaction using image analysis to quantify the void and crack content of the aggregates. Macroscopic free expansion was shown to be linked to this parameter, independent of the curing conditions [3]. We have extended this study with a wider range of aggregates, and confirmed the relationship (Fig. 1). The connection between microscopic observations and macroscopic measurements, simulated by the model, supports the hypothesis that damage is induced by growing gel pockets in the aggregates.

2. ASR models in literature

ASR models are frequently formulated at the material level for use in structure-level codes, and use empirical relationships [4–7]. Constructing models from semi-empirical relations requires extensive experimental campaigns such as in the theses of Poyet [5] and Larive [8], where sufficiently large datasets are produced which allow robust fitting. The curing conditions, temperature, stress, and relative humidity are varied, and the resulting evolution of expansion over time is measured as function of those parameters. The findings from such approaches are extensive and detailed, but are specific to each aggregate type. Coupling is often introduced between various parameters, even when these have no direct physical connection, such as aggregate size and alkali content.

Another approach consists in the development of analytical models. Relationships predicting the damage at the material level are derived from assumptions on the mode of reaction of the aggregates. These models frequently assume gel formation to occur preferentially at the interface between aggregate and paste [9,10]. The degradation of mechanical properties is described as coming from the ASR gel which first fills the pores and then induces expansion and cracks.

* Corresponding author.
E-mail address: cyrille.dunant@epfl.ch (C.F. Dunant).

0008-8846/$ – see front matter © 2009 Elsevier Ltd. All rights reserved.
doi:10.1016/j.cemconres.2009.07.024

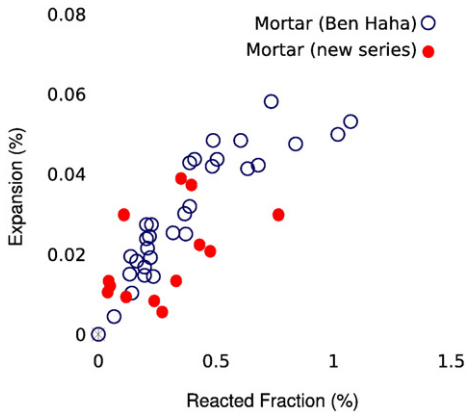

Fig. 1. Experimental relationship between measured free expansion and measured reacted fraction. Results from Ben Haha [3], as well as from the current study are reported.

Numerical models at the level of the microstructure are rare. For example, such models focus on the fracture mode of a single aggregate such as in the work of Çopuroğlu and colleagues [11], which computes crack propagation in a single aggregate using a lattice model.

Models can be formulated from phenomenological or mechanistic points of views. The lack of consensus about the origin of the degradation mechanism on one hand, and the difficulty of measuring the advance of the reaction rather than its consequences on the other hand make the formulation of experimentally based mechanistic models arduous. Nevertheless, there are some publications which relate macroscopic consequences to a measure of the reaction. Garcia and colleagues studied the evolution of the pore volume inside aggregates [12], and measured the evolution of the proportion of the various types of silica tetrahedra during the swelling. They propose a mechanism based on a diffuse reaction in the aggregates causing micro-cracking, and note that the relation between expansion and reaction is strongly influenced by the degradation state of the aggregates and paste. Ben Haha and colleagues linked the fraction of the aggregates which reacted to form ASR gel to macroscopic free expansion [3].

Whether the models be analytical, semi-empirical or numeric, they rely on underlying hypotheses about the degradation mechanism. The manifestation of the reaction has been shown by Ponce and colleagues to depend on the mineralogical nature of the aggregates [13]. Aggregates such as opal or vitreous volcanic rocks react from the surface, with a predominance of gel formation at the paste-aggregate interface. Mixed mineralogy aggregates, which are more common in the field, have reactive sites dispersed throughout their volume. A numerical framework capable of integrating the various microstructural manifestations of the reaction is therefore necessary to model ASR in general.

3. Experimental observations

Ben Haha monitored the expansion of concrete and mortars cast with moderately reactive aggregates at different temperatures and alkali levels [3]. This experimental study was extended by the current authors with different aggregates with more varied mineralogies. Polished sections were prepared for back-scattered electron microscopy observations at intervals.

The damage state of the aggregates was measured using the image analysis methodology developed by Ben Haha and co-workers on the images of the polished sections. The aggregates were first extracted from the image, then a threshold was applied to determine the area of voids and cracks in each aggregate. The ratio of aggregate surface to void surface was used as a direct measure of the reaction progress (Fig. 2).

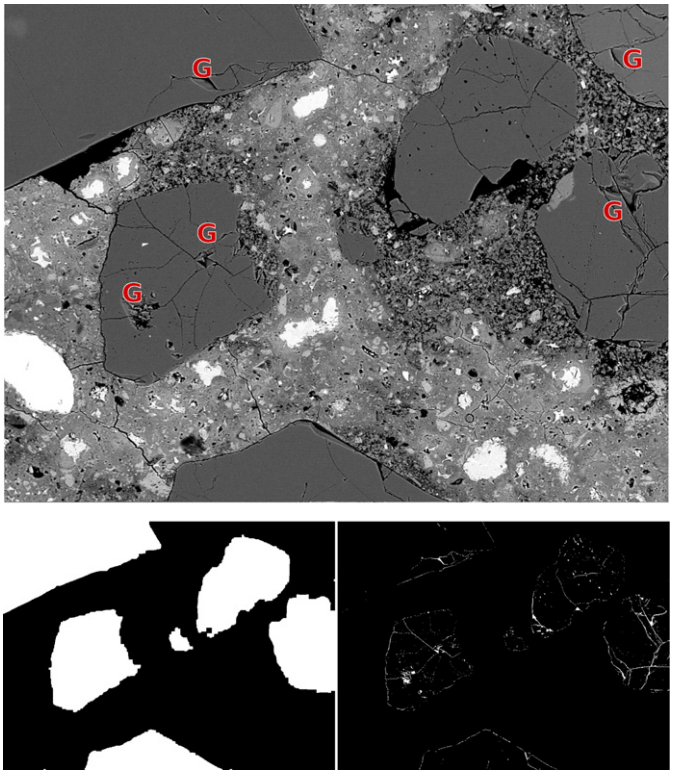

Fig. 2. Image analysis procedure used to extract the degree of reaction. The aggregates are extracted from the original image (top) as a mask (bottom left), and the damage in the aggregates is obtained through thresholding (bottom right). Gel packets are marked with G.

Ben Haha and colleagues had found a unique relation between expansion and reacted fraction. They derived a renormalisation function taking into account the aggregate fraction which allowed the comparison across samples with varying grain size distributions (Fig. 1). We confirmed this relationship with the new aggregates.

The reacted zones were found to be distributed throughout the aggregates. Similar observations were made on both concrete and mortar samples. This is consistent with what is reported in the work of Ponce and colleagues for mixed mineralogy aggregates [13]. These experimental observations served as a basis for the numerical model with the expansion of randomly distributed reactive zones randomly in the aggregates, inducing macroscopic expansion and damage.

4. Model

The microstructural model present here is based on the AMIE framework, which integrates a set of tools to provide the necessary components for the simulation of concrete at the microscale: geometry library, mesher, finite and extended finite element libraries [14], solvers, post-processors. It is optimised to integrate a number of enrichment sources much larger than that common in other available software [1,15].

For the simulation of ASR, a typical simulation is as follows. From a particle size distribution, aggregates are generated and placed in a sample. In each aggregate reactive zones are generated and placed. The framework then generates the discrete representation of the setup (Fig. 3). At each step, boundary conditions are applied, and the reactive zones are caused to expand. The damage caused by this expansion is computed, and the macroscopic properties are extracted. The process then repeats a specified number of steps.

To investigate in detail the effects of ASR at the meso-scale, an explicit numerical representation of many factors is required. This implies large simulations, namely a finely meshed standard mortar bar cross-section of 40 mm × 40 mm. Such large simulations are necessary as crack-paths within aggregates spanning the entire particle size distribution will be

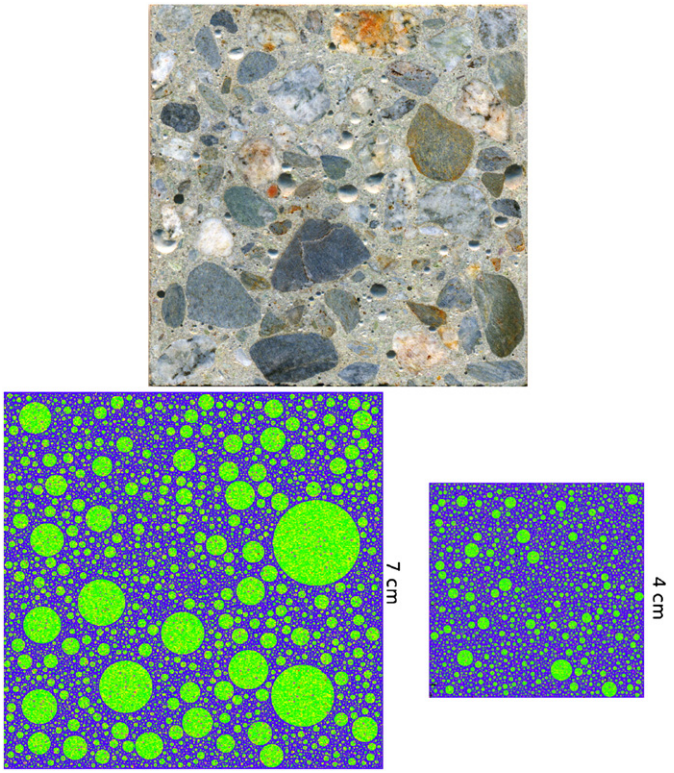

Fig. 3. Simulated concrete (centre) and mortar microstructures (right), compared to an actual slice (left).

produced; direct comparison of the simulations with experimental data is direct and furthermore features such as the wall effect at mould surface are also simulated.

Spherical aggregates are used for simplicity. Indeed, the PSD is known to affect the reaction, whereas no particular effect of shape has been identified. Also, the aggregate shape will have little effect because the reactive zones grow inside the aggregates. The microstructure is generated using a random packing algorithm, which allows a packing density of 63% of volume with aggregates to be achieved in a few seconds. The particle size distributions of the aggregates is taken from that of the real mortars and corrected for the three dimension to two dimension slicing effect. The ratio of largest to smallest aggregate is 50, which is a cut off at 200 μm.

The reactive zones are explicitly positioned within the aggregates. As these reactive zones are much smaller than the aggregates and growing as the reaction proceeds, meshing them would yield problems too large to solve in reasonable time. Therefore an XFEM representation for the growing reactive zones was chosen to allow their explicit representation, position, size and evolution. Although the framework is constructed to allow simulation in three dimensions it is not practical at present to manage the large amount of data required for such simulations at this resolution, therefore the current approach is restricted to two dimensions.

The mechanical properties of paste and aggregates (stiffness, critical stress) were obtained experimentally. The simulation of the intrinsic variability of the paste and aggregates is important to stabilise crack propagation, as well simulate crack initiation at local defects. Aggregates in ASR-affected structures exhibit variable mineralogies and so their mechanical properties will vary at the local level.

The influence of the varied nature of the aggregate is simulated by varying randomly the distribution of the mechanical properties of the elements making up the aggregates. This local variability is modelled by having the mechanical properties $\mathcal{P}$ of the elements follow a simple statistical law:

$$\mathcal{P} = \mathcal{P}_{\text{Prescribed}} \cdot (1-\xi) + \mathcal{P}_{\text{Prescribed}} \cdot \xi \cdot \omega \tag{1}$$

In this equation, ω is a random Weibull variable and the randomised fraction of the property, ξ, is set at 0.2; this fraction follows a Weibull law of mode $\mathcal{P}_{\text{Prescribed}}$. This factor was set to reproduce the experimental spread observed in mechanical tests.

The paste fills the space not occupied by the aggregates and has similarly randomised properties. Both aggregates and paste are assumed to be linear elastic, with damage. The finite element formulation for linear elasticity is implemented using the usual form (Eq. (2)).

$$\mathbf{K}_{ij}^{e} = \int_{e} \nabla h_i \mathbf{E}^{e} \nabla h_j \mathrm{d}e \tag{2}$$

In this equation e marks the element contribution, h_i is the ith shape function, $\mathbf{K}_{ij}^{e}$ the elementary contribution to the global stiffness matrix, for the ith and jth shape functions, $\mathbf{E}^{e}$ the element's Cauchy–Green stress tensor. The per-shape function formulation makes this formulation equally valid for extended finite elements.

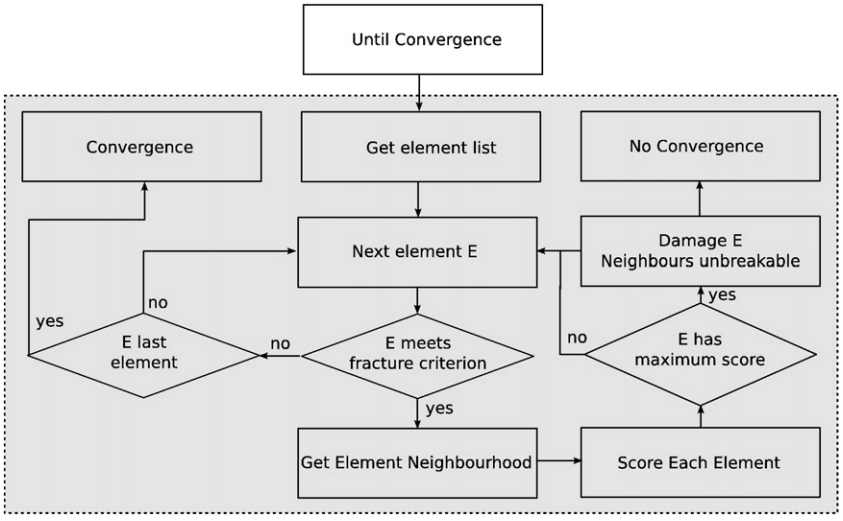

Fig. 4. Flow diagram of the algorithm which determines which element must be damaged. This method ensures that at each step of the cracking process the damage increment minimises the global energy. If the increment is small enough, this method effectively reproduces the damage history which corresponds to the global energy minimum.

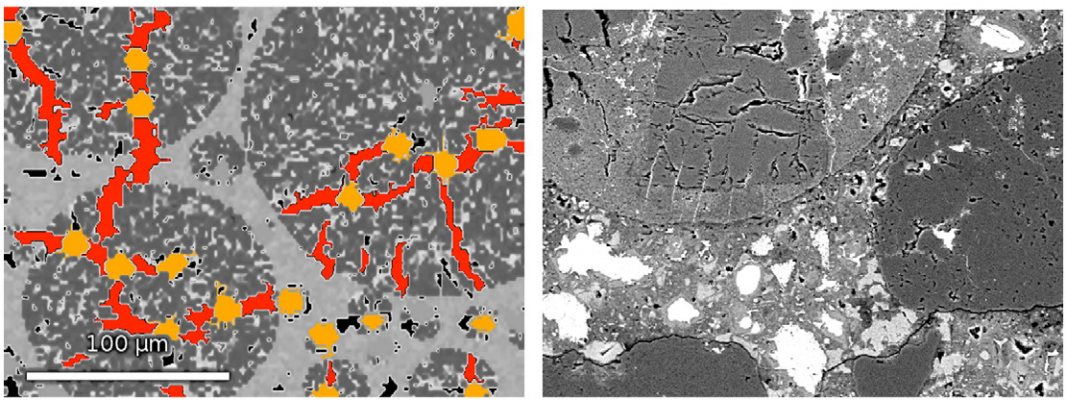

Fig. 5. Detail of a fracture pattern generated by the ASR model (left). For comparison, a micrograph at the same scale of an aggregate (right).

Once the microstructure has been generated, it is meshed conformantly using a Delaunay mesher, developed in-house around the core meshing algorithm from Devilier and colleagues [16]. The samples were finely meshed to capture the fracture pattern within the aggregates and the paste.

4.1. Damage model

Damage at the meso-scale is induced by a dense network of cracks. Because of the multiplicity of those cracks, special care must be taken that their propagation corresponds to a global energy minimum. The algorithm outlined in Fig. 4 ensures this is the case, even if multiple fracture criteria and damage mechanisms coexist. This approach leads to simulated fracture patterns which are qualitatively similar to the experimentally observed ones (Fig. 5).

Also, the more usual method of iterating on the load state to match the damage is not applicable, as the damage is induced by a load prescribed by the setup of the simulation. Thus, the fracture propagation to the point of equilibrium must be determined *a posteriori*, after the load has been set.

As both paste and aggregates can be considered quasi-brittle, we have opted for the following damage evolution law where the damage evolution parameter η is adjusted to the experimentally measured material parameters and ε is an arbitrarily small value.

$$d^{i+1} = \max(d^i + e^{\eta d^i}, 1-\varepsilon) \tag{3}$$

Where d is a factor such that the Young's modulus E is related to the original modulus by the Eq. (4).

$$E = (1-d)E_0 \tag{4}$$

The damage is incremented when a failure criterion is reached. The failure criterion used in our simulations is a modified Mohr–Coulomb criterion. It is reached when the maximum principal stress is beyond a critical value in tension or compression. Our choice of failure criterion was validated by the fact that it produces failure patterns which are morphologically identical to the experimentally observed ones.

To ensure that the damage is applied on a non-local basis, a neighbourhood is defined for each element which defines the density of elements which can be damaged at each step of the damage computation. A neighbourhood of the size of the average inter-aggregate distance yielded results closest to the experiments. To determine which elements should be damaged at each step of the damage computation loop, we defined a score which allows inter-element comparison. This score is based on the distance to the fracture surface defined by the criterion. In those simulations, the score s is calculated as defined in Eq. (5).

$$s = 1-\frac{\sigma_{\max}}{\sigma_{\text{crit}}} \tag{5}$$

4.2. Gel model

Microscopic observation of a wide range of mineralogically different aggregates consistently revealed the presence of ASR gel pockets in the aggregate.

The originality of our model lies in the fact that the gel pockets are explicitly considered, so the damage in the aggregates and paste emerges from the numerical setup of the meso-structure directly. The implementation of this feature required the use of modern developments in both numerical theory and numerical methods.

Gel pockets are modelled using a soft-discontinuity type of enrichment. This type of enrichment simulates a perfect contact between to materials of distinct mechanical properties. The enrichment function ϕ used was introduced by Moës and colleagues [15].

$$\phi(\mathbf{x}) = 1-|\mathbf{x}-\underset{\Gamma_{\text{gel}}}{proj}\,\mathbf{x}| \tag{6}$$

With Γ_{gel} the gel boundary, proj the projection operator, and $\mathbf{x}$ coordinates in the global system.

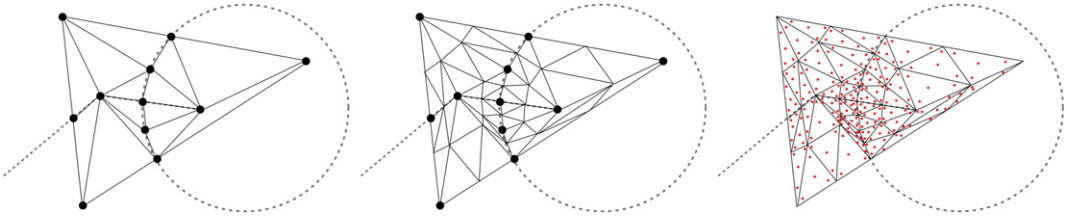

Fig. 6. Steps in the generation of a quadrature. A conformant mesh is generated as a function of the geometrical base of the enrichments. This mesh is refined using an adaptive quadtree algorithm. The Gauss points are kept, and the sub-mesh discarded.

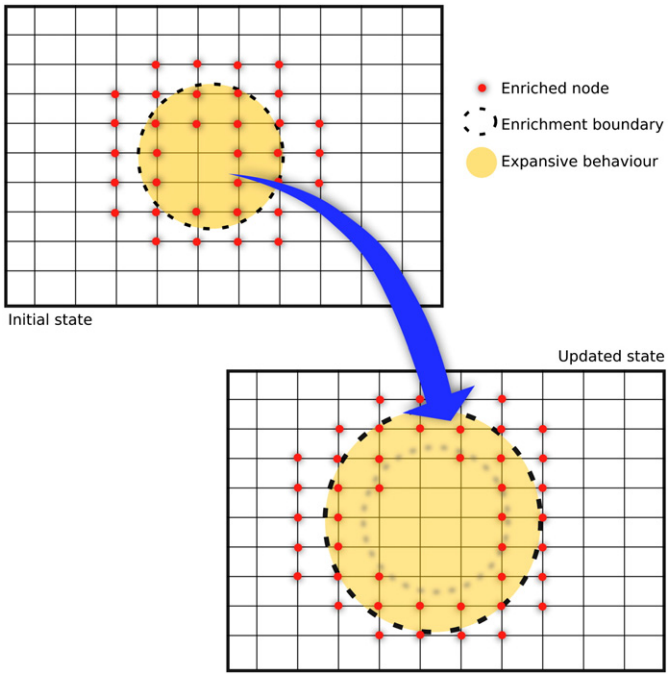

Fig. 7. Update of the enrichment scheme. The scheme is illustrated on a structured rectangular mesh for clarity, however, the mesh used in the simulations are triangular unstructured.

The integration step is performed by generating a temporary conformant tessellation of each enriched element. The generated mesh is then refined until convergence of the domain integral of the enrichment functions is reached. The final quadrature generated in this way is then used for the integration of the weak form defining the behaviour, and the temporary mesh is discarded (Fig. 6).

Using this approach, we can model the gel by taking into account the spatial distribution of the reactive zones, their size and the interface between the gel and the aggregates. The gel properties are assumed to be linear elastic with an imposed strain, as the gel is constrained by its surroundings until large amounts of damage have occurred. Using XFEM, we can accurately represent the geometry in each simulation step as illustrated on Fig. 7.

The gel mechanical properties are not well known, and experimental measures exhibit important variability in terms of the chemical nature of the gel [17] and its apparent mechanical properties [18–20]. However, the chemistry of the ASR gel, is close to that of C–S–H. For this reason, we have decided to assume that the gel is quasi-incompressible, with a Poisson ratio of 0.49997, that of water, and a stiffness which is a fraction of that of C–S–H [21], expressed in the figures as α. The gel was modelled as elastic and not visco-elastic because as it was assumed to be incompressible, the visco-elasticity would not have affected the results while the gel was fully restrained. Further, the experimental observations could be reproduced without the additional degree of freedom introduced by the visco-elasticity.

The free expansion of the gel is, like the mechanical properties, difficult to measure experimentally. However, it can be obtained by fitting the early part of the free expansion–damage curve. In the very early stages of the reaction, the damage from induced cracks is very little, and the expansion of the sample can be assumed to be elastic. From this we can obtain the expansive property of the gel which would result in this expansion. We found that a 50% volume expansion fits the experiments. The variability of the image analysis method at the early age of the reaction makes it difficult to be very precise about this value. However, the overall result of the simulation is not very sensitive to the value taken and 50% is also consistent with the stoichiometric volumetric ratio reported by Garcia and colleagues [12].

The strain of the gel, ε_{imp} is imposed as a virtual force on the nodes of the elements inside or cut by the gel pockets. The integration scheme is generated such that only the fraction of the element where the swelling takes place is accounted for (Eq. (7)).

$$\mathbf{f}_i = \int_{\Omega_{\text{gel}} \cap e} \nabla h_i \mathbf{E} \varepsilon_{\text{imp}} \mathrm{d}(\Omega_{\text{gel}} \cap e) \tag{7}$$

Ω_{gel}, the gel surface, e the element surface, h_i the shape function associated to the degree of freedom considered, $\mathbf{f}_i$ the associated force, $\mathbf{E}$, the Cauchy–Green stress tensor of the gel.

4.3. Reaction mechanism model

The model presented here is at present a chronic. The sample expansion is computed only against the degree of reaction, which is the part of aggregate which has reacted to form ASR gel. Thus the mechanical model cannot yet take into account such time-dependent behaviour as gel flow and paste creep depending on the curing conditions. As reaction could take weeks or years, creep may be important and we expect our model to predict expansions higher than the experimentally measured ones at the later stages of the reaction, as no relaxation mechanism is present other than cracking.

The gel is grown by steps in each aggregate until a preset percentage (3%) of the considered aggregate has reacted, at which point we stop the reaction in that aggregate. To verify the influence of gel growth capping per particle, we ran simulations where all gel pockets grow in the same

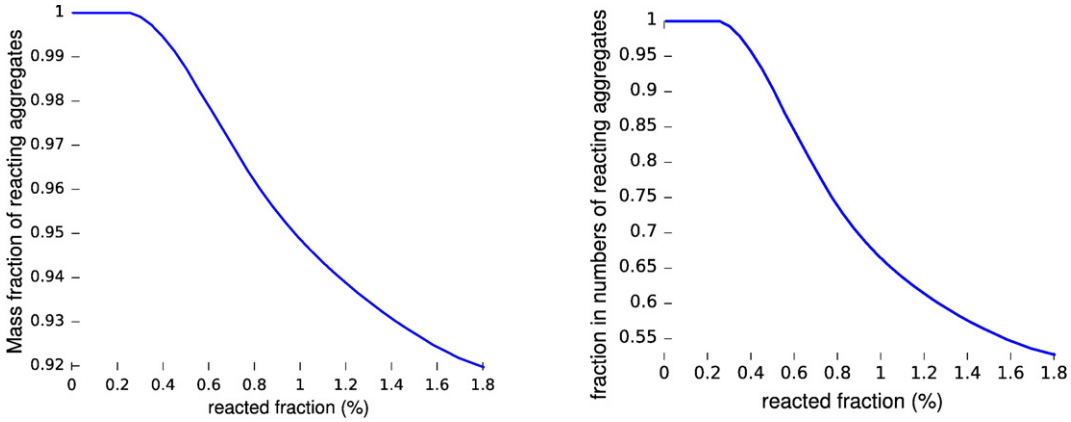

Fig. 8. Fraction of the mass of individual aggregates where the reaction has been stopped as a function of reaction advancement (left). Fraction of the number of individual aggregates where the reaction has been stopped as a function of reaction advancement (right).

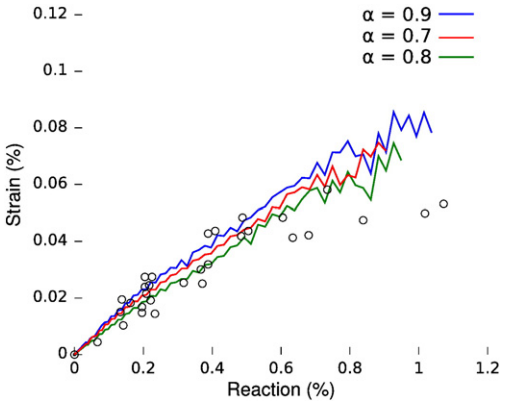

Fig. 9. Simulated expansion–reaction curve for mortar. The curves are not prolonged because a state is reached where the samples are not of a single piece anymore.

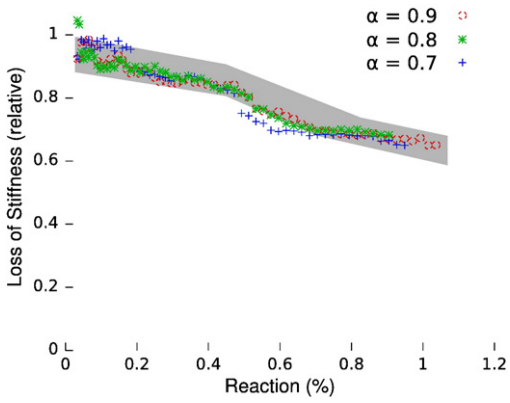

Fig. 11. Stiffness as a function of the progress of the reaction (left). The loss of stiffness as a function of expansion is compared to a range of reported values from Ben Haha (grey shade).

way, independent of their location. The gel is principally located in the larger aggregates, as they form the main fraction of aggregate volume. Thus, stopping the reaction in the smaller aggregates has little effect on the final expansion. However, the initial shape of the expansion–reaction curve is slightly affected.

By the end of the run nearly half of all aggregates have exhausted their expansion potential (Fig. 8). This effect can be simulated explicitly in our model as the full PSD is represented.

5. Results

5.1. Simulation of the free expansion of mortars

The simulated expansion–reaction curves follow the early part of the experimental dataset, but reach a plateau at higher expansions. The jitters observed in the simulated curves start at the onset of paste failure, which happens at the same reaction level as in the experiments. The higher final expansion can be explained by the absence of strain relaxation mechanisms in the paste other than crack propagation: there is no creep (Fig. 9).

As shown in Fig. 10, the measured damage and the actual reaction diverge. For this reason we have only simulated expansions up to 1% of reaction. At this level significant damage has occurred (Fig. 11), beyond what would have been considered critical in a structure.

The expansion–reaction curves obtained from simulation match the experiment well within the observed variability, with no fitting parameters other than the stiffness and free expansion of the gel. We found that the range of gel stiffness which could fit the experimental relationship is quite large: between 0.6 and 0.9 of that of C–S–H.

5.2. Prediction of the loss of mechanical properties

From the average stress and strain of the samples at each time point, we can compute the apparent stiffness of the sample, and thus link the advancement of the reaction to the damage level in the sample. These results are then compared to experimental values reported in the literature (Fig. 11).

The loss in stiffness is mostly due to the aggregates cracking, as the paste is mostly in compression, due to the dense aggregate packing, with stress levels below the elastic limit (Fig. 12). Tension is observed mostly in the aggregates around the gel pockets. This is consistent with microscopic observations which show extensive damage of the aggregates but nearly intact paste (Fig. 14). Paste failure occurs only when cracks from the aggregates reach the paste, thus increasing the tensile stress locally and initiating failure there. This also means that

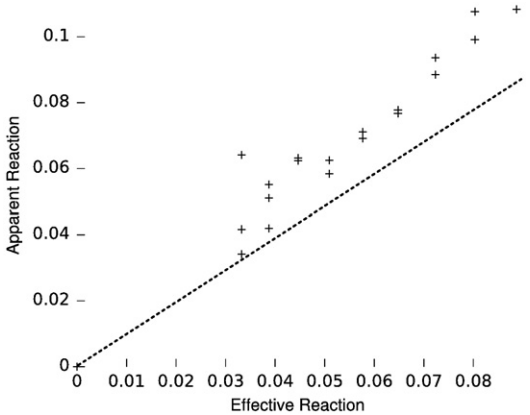

Fig. 10. Apparent reaction as a function of effective reaction. The dotted line is the line of equality.

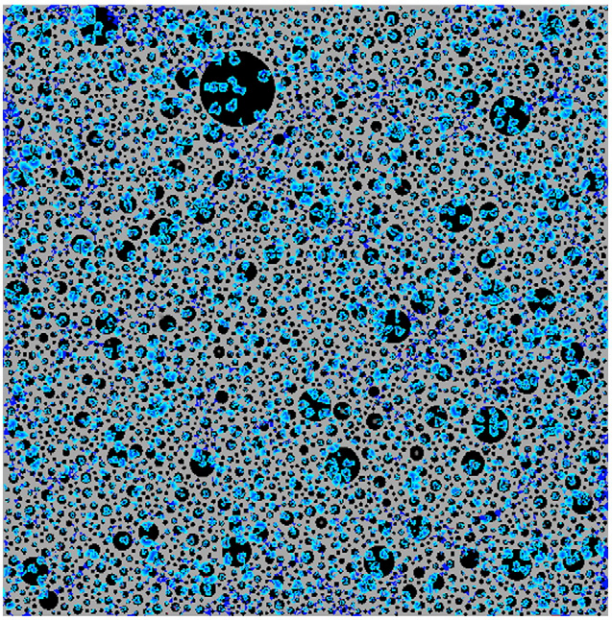

Fig. 12. Map of the sample zones which are in tension and compression. The zones in tension are where the ASR gel pockets are located — in the aggregates, whereas most of the rest of the sample is in compression, notably the paste.

the properties of the interfacial transition zone between paste and aggregate, which we have not at present included in our model will have negligible impact on the damage evolution.

The loss of stiffness predicted by the simulation is consistent with data reported in the thesis of Ben Haha [22], but is sensitive to the choice of gel properties at low reaction values.

5.3. Sensitivity to the various parameters

Several simulation campaigns were run to verify that our results are not sensitive to numerical effects. First we verified sensitivity to mesh size. The characteristic element size was halved, yielding four times as many elements, and the same simulation was run. The results are not significantly different when using a much finer mesh. This verifies both the XFEM model for the expansive zones and the energy-conservation of the damage model. The expansion values vary by only 2% at the final degree of reaction (e.g. at 1% expansion, the error is $\pm$ 0.02%).

Another second simulation campaign was run with a microstructure as dense as the packing algorithm allows. A mortar sample was generated with a packing density of 71%, larger than the value from the experimental mix design. The final expansions differed by only a relative amount of 6%, which is consistent with the increase in reactive material.

Finally we also verified the sensitivity to the variability of the local mechanical properties. We varied from 0.2 to 0.5 the weight ω (see Eq. (1)). Increase in variability lead to earlier cracking, but does not affect measurably the results.

6. Discussion

6.1. Correlation between damage and reaction

Image analysis cannot distinguish well between reaction (gel or voids) and damage (cracks): both appear as dark zones in the aggregate. In our simulations we compared the apparent reaction, as would be measured by the image analysis and the effective reaction, which is given as an input in the program. As expected, the apparent damage is larger than the effective reaction percentage. However they are close, and quasi-linearly related, if divergent. The cracks do not represent a significantly large volume of damage, compared to the volume of the gel pockets (Fig. 10).

The apparent expansion–reaction curve is less sensitive to the fit parameters than the real one (Fig. 13). This is explained by the strong link between damage and expansion, which is more direct than the link between expansion and reaction. This further explains the low variation observed experimentally across aggregate types and curing conditions. The noise apparent in the simulated damage–expansion curve is due to the healing effect of gel growing over fractured aggregate matter. This variation is consistent with experimental variability.

6.2. Expansion mechanism

The expansion–reaction curve exhibits three regimes: linear expansion, aggregate cracking and paste cracking (Fig. 14). These three regimes are illustrated by micrographs taken by Ben Haha: cracks are only visible in the paste after the aggregates have suffered significant degradation. The simulation shows that this is the result of four mechanisms: the expansion caused by the gel, the relaxation from the damage, the interaction between the gel zones, and the creep. The growth of the reactive zones can be measured as the reaction advances, and provides an insight into the expansion mechanism. In the first stage, as the gel progressively damages the aggregates, the expansion becomes less and less restrained until a plateau is reached, at this point the gel is essentially free to expand in the aggregates. This plateau comes to an end as the paste starts restraining further expansion. This evolution is mostly governed by the evolution of damage, and is not very sensitive to the gel stiffness parameter, but rather to gel localisation. It should be noted that the expansions at the end of the first stage are already well in excess of those likely to cause structural problems in large unreinforced structures such as dams.

As expected, the simulated expansion levels off at a higher point than the experimental ones (Fig. 13). This can be explained by the time-dependent visco-elastic behaviour of the gel and the creep of the paste not being modelled in these simulations, which leads to less strain relaxation than in real samples.

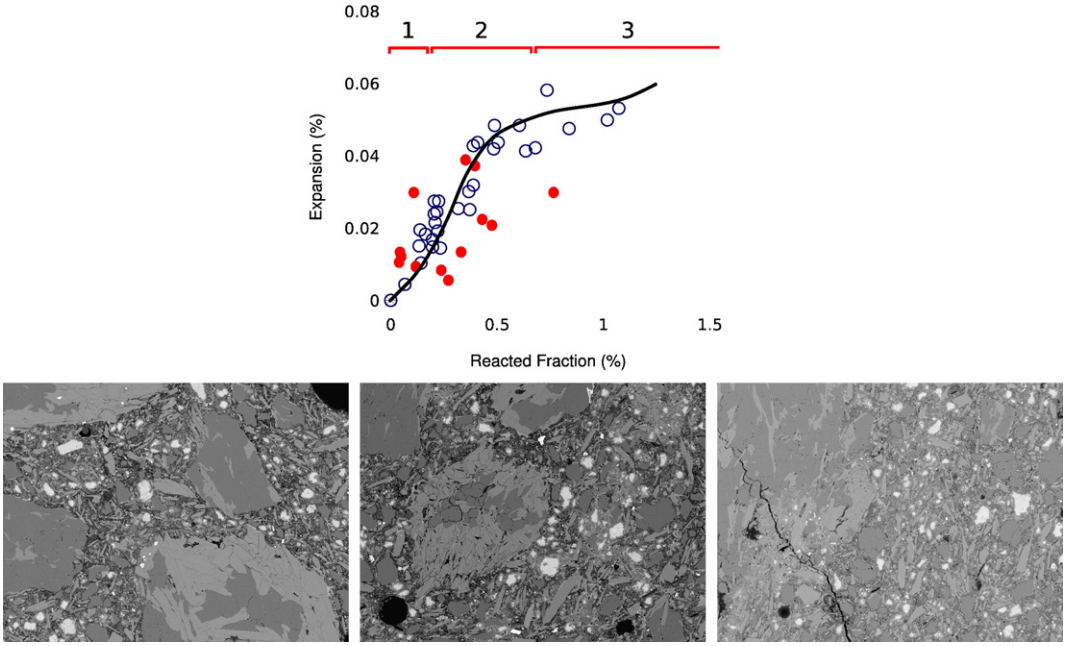

Fig. 13. Mechanism for expansion and degradation. (1) Elastic expansion; (2) Aggregate failure and gel pressure buildup; (3) Paste cracking. corresponding pictures at 7, 40 and 90 days taken by Ben Haha.

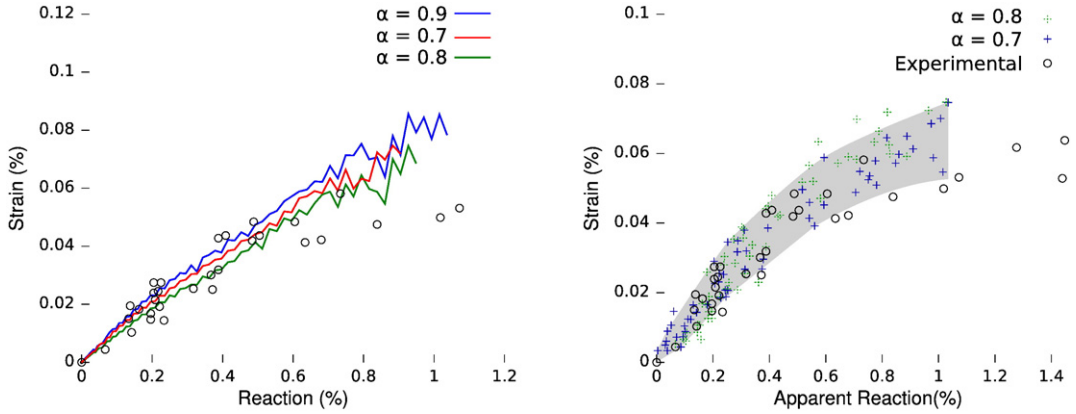

Fig. 14. Comparison between the real expansion–reaction curve (left) and the apparent one (right). The point where the expansions reach a plateau is higher than the experimentally measured values in both cases. This indicates that a relaxation mechanism is not taken into account in the simulations.

6.3. Comparison to other models

Various simplifications have been proposed for meso-scale modelling of ASR (Fig. 15). The simplest model applies a pseudo-thermal expansion for the aggregates as a source for the expansion. We found it possible to calibrate such model to fit the early part of the curve, using a linear correlation between the imposed strain and the degree of reaction. However, such a model does not capture the damage in the aggregates, and thus the loss in physical properties (Fig. 16).

The predictive nature of such a model is low, as the expansion of the aggregate must be computed as an empirical function of the degree of reaction. Such models have been used in the past to predict free expansion, using reduced particle size distributions. However the simulations demonstrates that such models are extremely dependent on the PSD of the aggregates, and exhibit very different damage patterns depending on the accuracy of the representation of the microstructure. Simplification of the PSD has consequences on the evolution of damage. A dense packing of aggregates causes all the paste to be in compression, whereas a reduced packing allows for higher shear levels in the paste, which then leads to cracking at lower levels of macroscopic expansion in those simulations.

When the local stress around the aggregates reaches a critical threshold, the sample undergoes critical failure. We found the critical failure to occur at the same imposed expansion, independently of the aggregate content.

The expansion–reaction curve observed experimentally exhibits different regimes: linear expansion, aggregate failure, paste failure (Fig. 14). The simplified model can capture the first and last regimes. When the local stress around the aggregates reaches a critical threshold, the sample undergoes catastrophic failure. The stress imposed by the aggregates needs to be fit with an empirical model which would include the effect of the damage in the aggregates. As such, this simplified model is incomplete if using only directly measured experimental values.

Another simple model for the reaction which has been proposed is that the gel is formed as a rim around the aggregate. This is notably consistent with observations made on dense aggregates. Such a microstructural makeup has never been explicitly simulated, but this vision of the reaction is used as the source of other semi-empirical models, such as the growing aggregate model described above. This model can be correlated to an advance of the reaction, as the gel localisation and amount are explicitly defined for each step of the reaction. To test this model, we implemented an enrichment scheme which could reproduce the two distinct interfaces between the aggregate and the gel, and between the gel and the paste.

Fig. 15. Three models for ASR-induced expansion. Homogenised aggregate expansion (left), gel rim expansion (centre), gel pockets expansion (right).

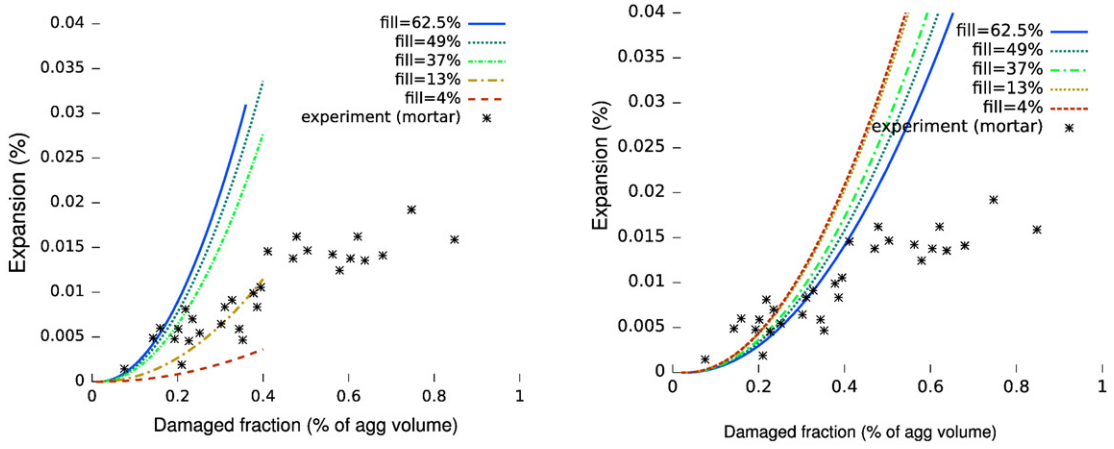

Fig. 16. Expansions predicted by a simplistic model, with varying cutoff points in the PSD (left). Expansions have been renormalised according to the aggregates content (right).

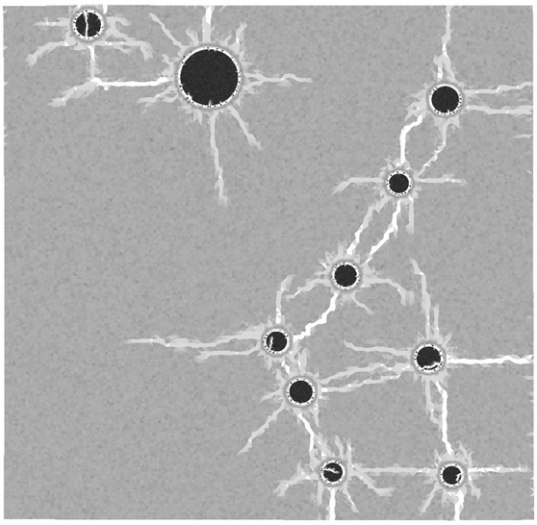

Fig. 17. Crack patterns produced by an expansive ring of gel formed around the aggregates.

This model is different from the precedent in that it explicitly affects the bond properties between aggregates and paste. We have not run simulation with full PSD, but have only run simulations with reduced amounts of aggregates. The fracture patterns obtained in such a setup show this model is not a good candidate to explain the ASR degradation in the case of composite aggregates: The cracks are located in the paste, while the aggregates remain largely intact, except for cracks initiating at the interface. Considerable decohesion between the aggregates and the paste is also observed (Fig. 17). In this setup, the aggregates crack due to the isostatic pressure imposed by the gel ring: splitting is apparent in some of the aggregates in the Fig. 17.

The simulations show that the macroscopic expansion and damage are strongly linked to the microstructural localisation of the reaction. Thus, the prediction of expansion from the advance of the reaction is only possible in models which simulated the direct consequences of ASR at the microstructure level.

7. Conclusion and perspectives

This paper presents a physically-based model of ASR, implemented and tested in a custom-developed FE framework. The model highlights the predominant effect of gel formation in the aggregates in the ASR degradation mechanism, notably damage in the aggregates themselves. The loss of mechanical properties can be wholly explained by the damage induced by the gel, and the model can be used to predict the evolution of mechanical properties. The model presented here showed robustness to the variation of the single fit parameter, apparent gel stiffness.

The implementation of simplified models commonly used to explain the mechanical effects of the reaction shows them to be inadequate to capture the physics of the phenomenon. The usual simplifications entail the transfer of the damage from the aggregates to the cement paste, which is experimentally observed to occur only during the advanced stages of the reaction. We also find that the shape of the free expansion/reaction curve cannot be captured by these models, unless it is imposed.

These simulations demonstrate the capacity of our finite element framework to perform well with an extremely high density of enrichments, which illustrates the robustness of our implementation. Because all elements of the phenomenon are explicitly formulated, it is possible, using this model to vary the boundary conditions and for example test the effect of mechanical restraint on the expansion.

Future work involves coupling the model with a diffusion mechanism for the alkali ions, and the introduction of time-dependent creep, which would serve as a base for a kinetic simulation of ASR.

Acknowledgement

We would like to thank the Swiss Federal Office of Energy for their support, financial or otherwise.

References

[1] C. Dunant, P.N. Vinh, M. Belgasmia, S. Bordas, A. Guidoum, Architecture tradeoffs of integrating a mesh generator to partition of unity enriched object-oriented finite element software, Revue Européenne de Mécanique Numérique 16 (2007) 237–258.
[2] S. Bordas, V.P. Nguyen, C. Dunant, H. Nguyen-Dang, A. Guidoum, An extended finite element library, International Journal for Numerical Methods in Engineering 71 (2007) 703–732.
[3] M. ben Haha, E. Gallucci, A. Guidoum, K.L. Scrivener, Relation of expansion due to alkali silica reaction to the degree of reaction measured by SEM image analysis, Cement and Concrete Research 37 (8) (2007) 1206–1214.
[4] B. Capra, J.-P. Bournazel, Modeling of induced mechanical effects of alkali–aggregate reactions, Cement and Concrete Research 28 (2) (1998) 251–260.
[5] S. Poyet, Etude de la dégradation des ouvrages en béton atteints par la réaction alcali–silice: Approche expérimentale et modélisation numérique multi-échelles des dégradations dans un environnement hydro-chemo-mécanique variable, Ph.D. thesis (2003).
[6] E.M.R. Fairbairn, F.L.B. Ribeiro, L.E. Lopes, R.D. Toledo-Filho, M.M. Silvoso, Modelling the structural behaviour of a dam affected by alkali–silica reaction, Communications in Numerical Methods in Engineering 22 (1) (2005) 1–12.
[7] S. Multon, F. Toutlemonde, Effect of applied stresses on alkali–silica reaction-induced expansions, Cement and Concrete Research 36 (5) (2006) 912–920.
[8] C. Larive, Moyens et Méthodes d'Essai, Études et recherches des laboratoires des ponts et chaussées, 1998 Ch. 3.
[9] T. Ichikawa, M. Miura, Modified model of alkali–silica reaction, Cement and Concrete Research 37 (9) (2007) 1291–1297.
[10] Z.P. Bažant, A. Steffens, Mathematical model for kinetics of alkali–silica reaction in concrete, Cement and Concrete Research 30 (3) (1999) 419–428.
[11] O. Çopuroğlu, E. Schlangen, Modelling of effect of ASR on concrete microstructure, Key Engineering Materials 348 (2007) 809–812.
[12] E. Garcia-Diaz, J. Riche, D. Bulteel, C. Vernet, Mechanism of damage for the alkali–silica reaction, Cement and Concrete Research 36 (2) (2006) 395–400.
[13] J. Ponce, O. Batic, Different manifestations of the alkali–silica reaction in concrete according to the reaction kinetics of the reactive aggregate, Cement and Concrete Research 36 (6) (2006) 1148–1156.
[14] I. Babuška, I. Melenk, Partition of unity method, International Journal for Numerical Methods in Engineering 40 (4) (1997) 727–758.
[15] N. Moës, M. Cloirec, P. Cartraud, J. Remacle, A computational approach to handle complex microstructure geometries, Communications in Numerical Methods in Engineering 192 (29) (2003) 3163–3177.
[16] O. Devillers, S. Meiser, M. Teillaud, Fully dynamic Delaunay triangulation in logarithmic expected time per operation, Computational Geometry Theory and Application 2 (2) (1992) 55–80.
[17] C. Tambelli, J. Schneider, N. Hasparyk, P.J. Monteiro, Study of the structure of alkali–silica reaction gel by high-resolution NMR spectroscopy, Journal of Non-Crystalline Solids 352 (32) (2006) 3429–3436.
[18] A. Binal, The determination of gel swelling pressure of reactive aggregates by ASGPM device and a new reactive-innocuous aggregate decision chart, Construction & Building Materials 22 (1) (2008) 1–13.
[19] J.E. Dolbow, E. Fried, H. Ji, Chemically induced swelling of hydrogels, Journal of the Mechanics and Physics of Solids 52 (1) (2004) 51–84.
[20] M. Kawamura, K. Iwahori, ASR gel composition and expansive pressure in mortars under restraint, Cement & Concrete Composites 26 (1) (2004) 47–56.
[21] G. Constantinides, F.-J. Ulm, The effect of two types of C–S–H term on the elasticity of cement-based materials: results from nanoindentation and micromechanical modeling, Cement and Concrete Research 34 (1) (2004) 67–80.
[22] M. Ben Haha, Mechanical effects of alkali silica reaction in concrete studied by SEM-image analysis, Ph.D. thesis (May 2006).